CHEMISTRY OF MATERIALS
Cite This: Chem. Mater. 2018, 30, 5743−5749
Article
pubs.acs.org/cm

Molecular Engineering of Bandgaps in Covalent Organic Frameworks

Xing Li,[†,‡] Qiang Gao,[†] J. Aneesh,[§] Hai-Sen Xu,[†] Zhongxin Chen,[†,‡] Wei Tang,[⊥] Cuibo Liu,[†] Xiangyan Shi,[∥] K. V. Adarsh,[§] Yixin Lu,*[,†,‡] and Kian Ping Loh*[,†,‡]

[†]Department of Chemistry, National University of Singapore, 3 Science Drive 3, Singapore 117543

[‡]Graduate School for Integrative Sciences & Engineering (NGS), National University of Singapore 28 Medical Drive, Singapore 117456

[§]Department of Physics, Indian Institute of Science Education and Research, Bhopal 462066, India

[⊥]Institute of Materials Research and Engineering, A*STAR, 2 Fusionopolis Way, Innovis, Singapore 138634

[∥]School of Physical and Mathematical Sciences, Nanyang Technological University, 21 Nanyang Link, Singapore 637371

Supporting Information

ABSTRACT: Two-dimensional (2D) covalent organic frameworks (COFs) are an emerging class of porous materials with potential for wide-ranging applications. Intense research efforts have been directed at tuning the structure and topology of COF, however the bandgap engineering of COF has received less attention, although it is a necessary step for developing the material for photovoltaic or photonic applications. Herein, we have developed an approach to narrow the bandgap of COFs by pairing triphenylamine and salicylideneaniline building units to construct an eclipsed stacked 2D COF. The ordered porous structure of 2D COF facilitates a unique moisture-triggered tautomerism. The combination of donor−acceptor charge transfer and tautomerization in the salicyclidineaniline unit imparts a large bandgap narrowing for the COF and turns it color to black. The synthesized COF with donor−acceptor dyad exhibits excellent nonlinear optical properties according to open aperture Z-scan measurements with 532 nm nanosecond laser pulses.

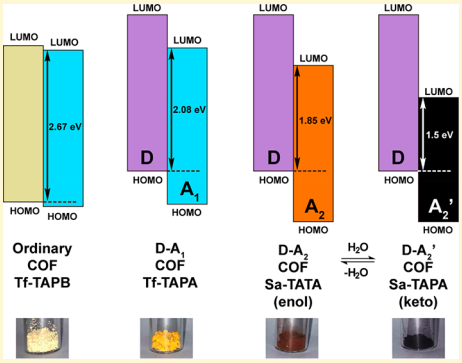

INTRODUCTION

Covalent organic frameworks (COFs) are molecular Legos that allow the precise integration of small organic building units into extended, porous, crystalline architectures via covalent linkage.[1−5] Well-designed COF can be used in wide-ranging applications such as catalysis,[6−10] gas storage,[11−13] optoelectronics,[14−16] solid-state fluorescence,[17,18] sensing,[19−21] solid electrolyte[22] and chemical removal.[23,24] Generally, most reported 2D COFs which are linked by boronate ester or imine linkages have large bandgaps[25] due to their short π conjugation lengths. Interest is now emerging on the bandgap engineering of COFs by integrating porphyrin,[26] phthalocyanine,[27,28] thiophene, or indigo-based building blocks.[16] From a conceptual viewpoint, the use of such building units does not provide a convincing case for how the 2-D framework structure allows additional bandgap narrowing since the building blocks already possess intrinsic narrow bandgaps in their molecular states. Besides, their synthesis is challenging and highly toxic reagents such as organotin compounds are required.

COFs covalently extend the building units into highly ordered architectures with controlled topologies such as two-dimensional (2D),[29] three-dimensional (3D),[30] and even woven structures,[31,32] thus should give rise to colligative properties that are different from small molecules or randomly bonded networks. Taking the cue from bandgap narrowing strategy used in the synthesis of polymers in photovoltaic applications, electron donor−acceptor pairs (dyads) can be incorporated in 2D COFs to form periodic donor−acceptor structure. Salicylideneaniline is potentially a good electron acceptor due to its photo- and thermochromism via reversible proton tautomerization.[33−36] Its enol-keto tautomerization in the free molecule state upon heating or UV light irradiation is accompanied by a redshift in absorption (Supporting Information, SI, Scheme S2) and has been well studied. Recently, we discovered that when salicylideneaniline is incorporated into a COF framework, exposure to moisture alone can trigger tautomerization.[23] We rationalize this by the ordered layered stacking environment in COF that facilitates proton transfer in the presence of water.

Herein, we report a facile approach to tune the bandgaps in COFs by taking advantage of this tautomerization. Starting from a COF with no dyad features, we can tune the bandgap from 2.67 to 2.08 eV by introducing triphenylamine as the

Received: June 18, 2018
Revised: July 31, 2018
Published: July 31, 2018

DOI: 10.1021/acs.chemmater.8b02560
Chem. Mater. 2018, 30, 5743−5749

donor unit. By adding an acceptor unit in the form of the salicylideneaniline moiety, the bandgap can be further narrowed to 1.5 eV with a broadband absorption up to 825 nm (Figure 1). The salicylideneaniline COF displays reversible

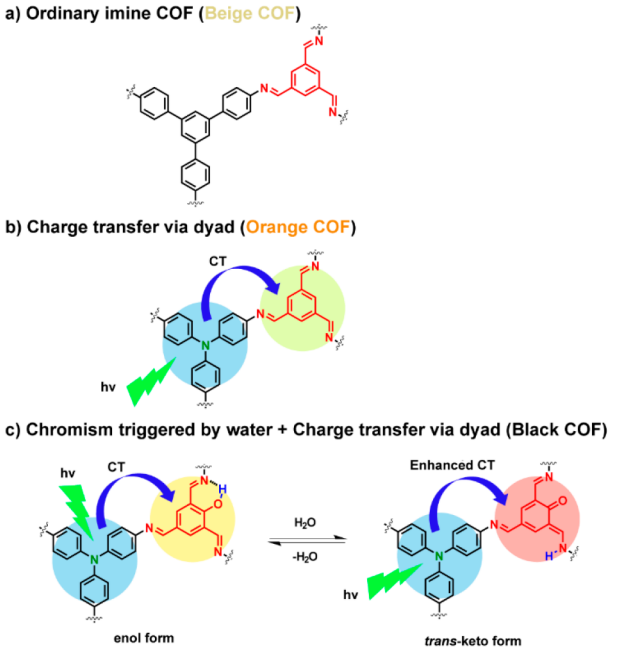

Figure 1. Synthetic strategy to achieve low bandgap COFs.

water-vapor-triggered chromism from red to black color. Interestingly, the dyad COF exhibits ultrafast nonlinear optical (NLO) response with an optical limiting behavior that competes with 2D materials such as graphene and molybdenum sulfide, suggesting that COF can be a new class of nonlinear optical (NLO) material.

EXPERIMENTAL SECTION

Synthesis of Sa-TAPA COF. To a mixture of 2,4,6-triformylphenol (0.1 mmol, 17.8 mg) and tris(4-aminophenyl)amine (0.1 mmol, 29 mg) was added with *n*-butanol (1 mL), *o*-DCB (1 mL), and 6 M AcOH (aq, 0.2 mL) in a 10 mL Schlenk tube (15 × 80 mm^2). The suspension was sonicated for 5 min, then flash frozen at 77 K, and degassed under freeze−pump−thaw for three cycles. The tube was sealed and heated at 120 °C for 7 days. The precipitate was exchanged with anhydrous THF (5 mL) for 6 times and dried under vacuum for overnight to afford a red color solid (39 mg, 94%). Anal. Calcd for $(C_{27}H_{18}N_4O{\cdot}6.8\ H_2O)_n$: C 60.39; H 5.93; N 10.43; O 23.24; found: C 60.29; H 3.15; N 10.56.

Synthesis of Tf-TAPA COF. To a mixture of 1,3,5-triformylbenzene (0.1 mmol, 16.2 mg) and tris(4-aminophenyl)amine (0.1 mmol, 29 mg) was added with 1,4-dioxane (1 mL), mesitylene (1 mL), and 6 M AcOH (aq, 0.2 mL) in a 10 mL Schlenk tube (15 × 80 mm^2). The suspension was sonicated for 5 min, then flash frozen at 77 K, and degassed under freeze−pump−thaw for three cycles. The tube was sealed and heated at 120 °C for 7 days. The precipitate was exchanged with anhydrous THF (5 mL) for 6 times and dried under vacuum for overnight to afford a yellow color solid (36 mg, 92%). Anal. Calcd for $(C_{27}H_{18}N_4{\cdot}3.35\ H_2O)_n$: C 70.68; H 5.43; N 12.21; O 11.68; found: C 71.49; H 4.22; N 11.4.

Synthesis of Tf-TAPB COF. A modified method was used to synthesize Tf-TAPB COF.[37,38] To a mixture of 1,3,5-triformylbenzene (0.1 mmol, 16.2 mg) and 1,3,5-tris(4′-aminophenyl)benzene (0.1 mmol, 35.1 mg) was added with 1,4-dioxane (1 mL), mesitylene (1 mL) and 6 M AcOH (aq, 0.2 mL) in a 10 mL Schlenk tube (15 × 80 mm^2). The suspension was sonicated for 5 min, then flash frozen at 77 K, and degassed under freeze−pump−thaw for three cycles. The tube was sealed and heated at 120 °C for 7 days. The precipitate was exchanged with anhydrous THF (5 mL) for 6 times and dried under vacuum for overnight to afford a beige color solid (46 mg, 97%). Anal. Calcd for $(C_{33}H_{21}N_4{\cdot}1.9\ C_4H_8O{\cdot}2\ H_2O)_n$: C 76.42; H 6.27; N 8.66; O 8.65; found: C 74.36; H 5.15; N 7.55.

Characterization. Powder X-ray diffraction patterns were collected on a Bruker D8 Focus Powder X-ray diffractometer using Cu Kα radiation (40 kV, 40 mA) at room temperature. Gas sorption analysis was performed on Quantachrome Instruments Autosorb-iQ (Boynton Beach, Florida U.S.A.) with extra-high pure gases. The

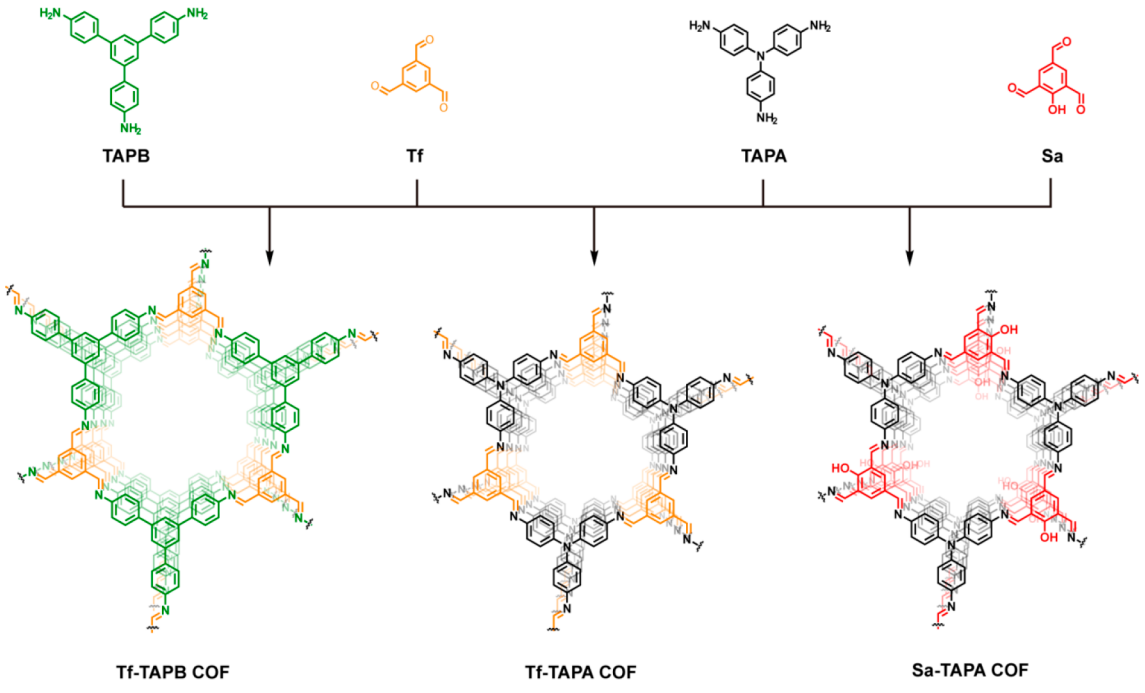

Figure 2. Precursors used for the synthesis of Tf-TAPB, Tf-TAPA, and Sa-TAPA COFs.

DOI: 10.1021/acs.chemmater.8b02560
Chem. Mater. 2018, 30, 5743−5749

samples were activated and outgassed at 120 °C for 8 h before measurement. The Brunauer–Emmett–Teller (BET) surface area and total pore volume were estimated using the N_2 sorption isotherms at 77 K, and the pore size distribution was calculated using Non-Local Density Functional Theory (NL-DFT, a carbon model containing slit/cylindrical pore) model in the Quantachrome ASiQwin 5.0 software package. Solid-state NMR experiments were performed on a 14.1 T Bruker Advance III NMR instrument equipped with a 4 mm H/N–P MAS probe. 1D ^{1}H-^{13}C CP-MAS NMR spectra were collected with 14 kHz MAS spinning frequency, and the variable temperature was kept at 296 K. FT-IR spectra were recorded on a Bruker vertex 80v spectrometer under vacuum. UV–vis–NIR spectra were measured using Shimadzu UV-3600 UV–visible–NIR spectrophotometer with an integration sphere setup. For the cyclic voltammetry measurement, the working electrode was prepared by dropcasting an ethanol suspension of respective COF, carbon black, and polytetrafluoroethylene (PTFE) (2:7:1 by weight) onto a glassy carbon electrode. The electrolyte was tetrabutylammonium hexafluorophosphate (0.1 M, acetonitrile). The counter and reference electrode were Pt wire and Ag/AgNO3. Ferrocene was used as a standard to calculate the energy levels vs vacuum.

RESULTS AND DISCUSSION

To demonstrate the role of dyad and proton tautomerization in narrowing the bandgap, the following COFs were synthesized:

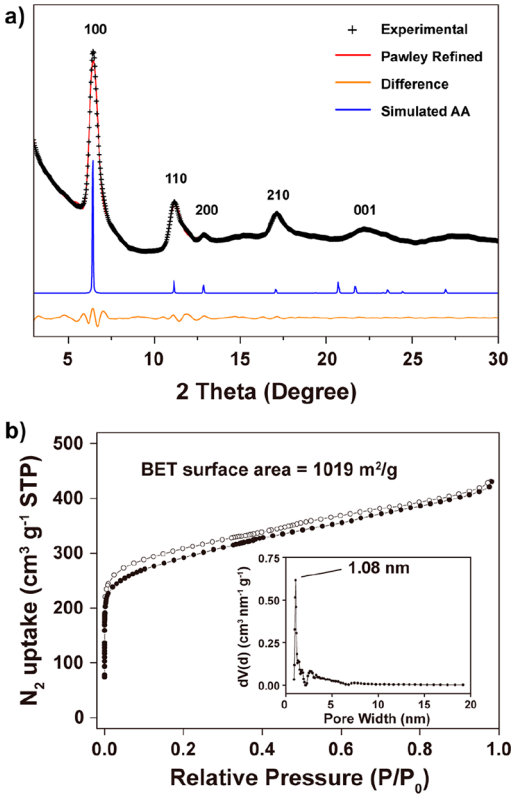

Figure 3. Characterizations of Sa-TAPA COF. (a) PXRD Patterns of Sa-TAPA COF (black: experimental; red: Pawley refined; blue: simulated eclipse stacking; yellow: difference between experimental and Pawley refined PXRD patterns). (b) Nitrogen sorption isotherm of Sa-TAPA COF (77 K, inset: pore size distribution).

Tf-TAPB with no dyad structure, Tf-TAPA with dyads but incapable of enol-keto tautomerization, and Sa-TAPA with both dyad and salicylidene units (Figure 2). One of the COF building unit, 2,4,6-triformylphenol (Sa), was synthesized in gram scale from phenol in one step via a Duff reaction; while

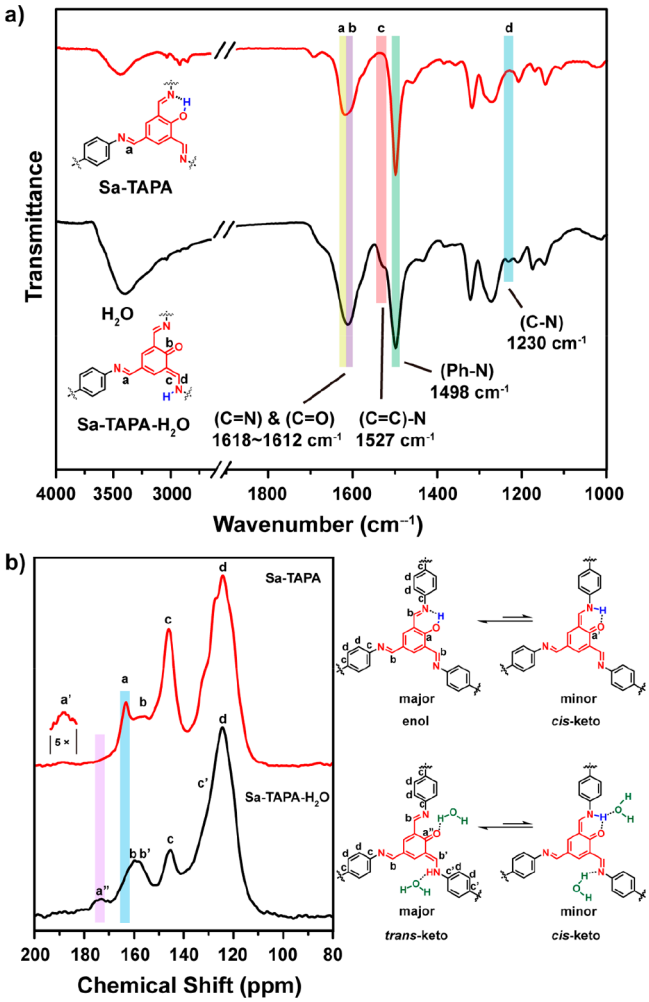

Figure 4. Moisture-triggered reversible proton tautomerization of Sa-TAPA COF. (a) FT–IR spectra of dry Sa-TAPA COF and moisture adsorbed Sa-TAPA-H_2O COF. (b) Solid-state CP/MAS ^{13}C NMR spectra of Sa-TAPA COF and Sa-TAPA-H_2O COF.

the other building unit, tri(4-aminophenyl)amine (TAPA), was commercially available and used without further purification. The black COF, namely Sa-TAPA COF, was prepared via solvothermal condensation of a mixture of Sa and TAPA in a 5:5:1 (v/v) solution of *o*-dichlorobenzene, *n*-butanol, and 6 M aqueous acetic acid. The complete consumption of the monomers was confirmed by the Fourier transform infrared (FT–IR) spectra with the disappearance of amino N–H stretching at 3404 and 3332 cm^{-1} and aldehyde C=O stretching at 1690–1660 cm^{-1}; meanwhile, the formation of imine bonds in the as-prepared COF was also verified by the imine C=N stretching band at 1618 cm^{-1} (SI Figure S1).

The crystalline structure of Sa-TAPA COF was confirmed by powder X-ray diffraction (PXRD) and simulation experiments (Figure 3a). The PXRD pattern exhibits a major peak at 6.44° with four minor peaks at 11.17°, 12.87°, 17.12°, and 22.20°, which are assigned to (100), (110), (200), (210), and (001) facet, respectively. The most intense (100) peak displays a full width half-maximum of 0.5°, which reflects the good crystallinity of the material. The eclipsed stacking (AA) structure of the Sa-TAPA COF was modeled using Focite Module in Material Studio version 2016. The simulated PXRD pattern agrees well with the experimental results, confirming

DOI: 10.1021/acs.chemmater.8b02560
Chem. Mater. 2018, 30, 5743–5749

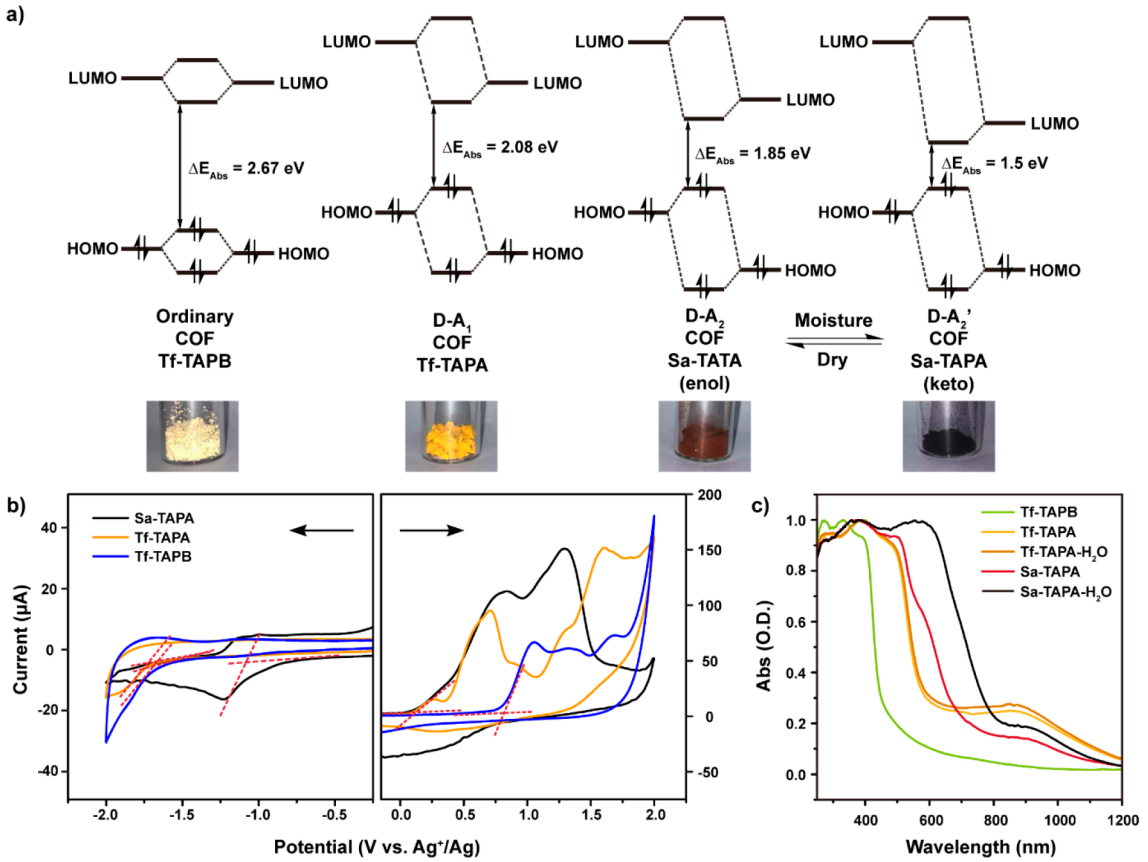

Figure 5. Band gaps of three COFs. (a) Energy level diagrams of Tf-TAPB, Tf-TAPA, and Sa-TAPA (dry and moisture-adsorbed) COFs. (b) Cyclic voltammetry of Sa-TAPA, Tf-TAPA, and Tf-TAPB (left: negative scan; right: positive scan). (c) UV−vis−NIR absorption spectra of Tf-TAPB, Tf-TAPA (dry and wet), and Sa-TAPA (dry and wet) COFs.

the eclipsed stacking structure of Sa-TAPA COF. The Pawley refinement also displays a good match to the experimental result with R_{wp} = 2.68% and R_p = 1.94%, and a small difference between the refined and experimental PXRD patterns. On the basis of above results, Sa-TAPA COF adopts eclipse stacking with a unit cell belonging to *P*3 space group where $a = b =$ 16.05 Å, c = 4.15 Å, $\alpha = \beta = 90°$, and $\gamma = 120°$.

The permanent porosity of Sa-TAPA COF was further studied via nitrogen sorption experiment at 77 K. The N_2 sorption exhibits a reversible type I isotherm, suggesting a uniform and well-ordered microporous structure of the material (Figure 3b). The Brunauer−Emmett−Teller (BET) surface area of Sa-TAPA COF is calculated to be 1019 $m^2\ g^{-1}$, with a total volume of 0.67 $cm^3\ g^{-1}$ at P/P_0 = 0.98. On the basis of nonlocal density functional theory (NLDFT), a narrow pore size distribution is obtained with an average pore width of 1.08 nm, which is consistent with the theoretical value of 1.18 nm based on the refined crystal structure.

The moisture-triggered reversible proton tautomerization of Sa-TAPA COF was monitored by Fourier Transform Infrared Spectroscopy (FT−IR) (Figure 4a).). The band at 1618−1612 cm^{-1} is mainly attributed to contributions from the C═N stretching of the imine linkage with a minor component due to the C═O stretching of the ketone group.[39] Using the C−N stretching of phenylamine fragment at 1498 cm^{-1} as a reference band, when the COF sample is exposed to moisture, the band at 1618−1612 cm^{-1} increases in absorption intensity, which is due to the convolution of vibrational modes from C═N stretching of the imine linkage to C═O stretching of the ketone group. This suggests the population of keto form increases when water is adsorbed. Moreover, the increase in the intensities of bands at 1527 and 1230 cm^{-1}, which are assigned to C═C stretching and C−N stretching of the keto-enamine group respectively, also confirms the formation of keto tautomers in Sa-TAPA COF. Notably, after drying Sa-TAPA-H_2O, the FT−IR spectrum reverts to its original form, thereby confirming the reversible tautomerization process (SI Figure S1). UV−vis absorption spectra reveal that the absorption edge redshifts from 670 to 825 nm when the COF adsorbs moisture. On the basis of experimental[33−35] and simulation[40] studies on small molecules of salicylideneaniline, the enol and *cis*-keto have similar absorptions due to their rather similar structures, while the *trans*-keto form gives a larger redshift in absorption due to the breaking of intramolecular hydrogen bonding. Thus, we propose the major tautomer in the moisture-adsorbed Sa-TAPA-H_2O is the *trans*-keto form.

Solid-state CP/MAS ^{13}C NMR further confirms the involvement of water in proton tautomerism (Figure 4b). At dry state, Sa-TAPA COF mainly exists in the enol form, and only a minority is in the *cis*-keto form. This is supported by the major peak at 163.3 ppm (a, phenol C) and the minor peak at 188.7 ppm (a′, conjugated C═O). When Sa-TAPA adsorbs water to form Sa-TAPA-H_2O, the COF mainly exists in the keto form. This is verified by the disappearance of phenol C peak at 163.3 ppm and the increased intensity of conjugated carbonyl C peak at 173.7 ppm (a″). The upfield shift of the carbonyl C peak is due to the water-induced hydrogen bonding

DOI: 10.1021/acs.chemmater.8b02560
Chem. Mater. 2018, 30, 5743−5749

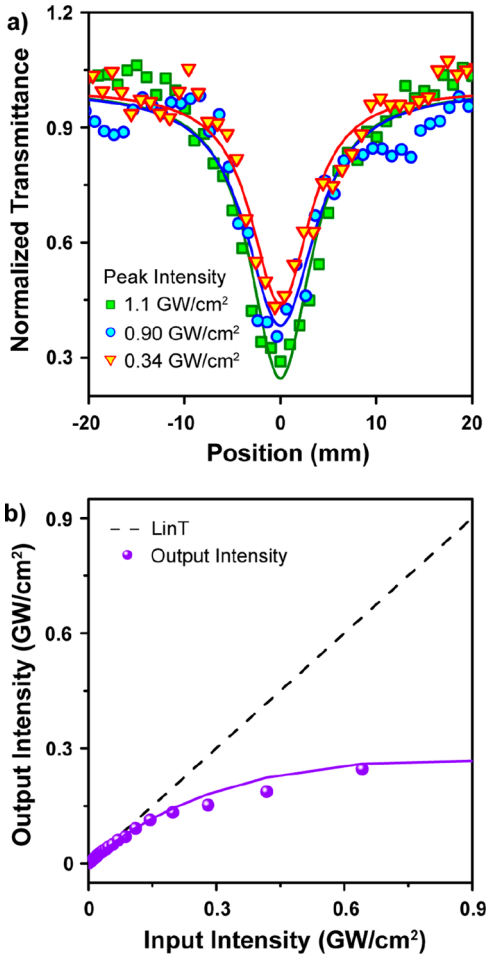

Figure 6. Optical limiting effect of Sa-TAPA COF dispersion in acetone probed by 532 nm nanosecond. (a) Open-aperture Z-scan plot of normalized transmittance against sample position. (b) Plot of output intensity against input intensity of laser. The light transmittance and output intensity are normalized by the linear transmittance of 20%.

interaction. Previous study showed that hydrogen bonding can result in significant change of chemical shift of carbonyl C in the solid state.[41]

Accordingly, we propose a mechanism for the reversible proton tautomerism in our synthesized COF (SI Figure S10). Sa-TAPA exists mainly in the enol form at dry state while it tautomerizes to the *cis*-keto form via intramolecular proton transfer in the six-membered ring. Upon water absorption, Sa-TAPA-H_2O further tautomerizes to *trans*-keto form. When salicylideneaniline unit exists as small molecules, the *cis*−*trans* keto tautomerization requires flipping of C═C bond, which has to be activated by UV-irradiation. The tautomerization energy barrier can be efficiently lowered when the salicylidene units are immobilized into the rigid framework of highly ordered 2D COF. We explain this by the fact that when water is adsorbed into the one-dimensional channels of Sa-TAPA, it facilitates proton transport from the *cis*-imine nitrogen to the *trans* position. This process is reversible; when water is removed from Sa-TAPA-H_2O, the COF returns to the enol form, which is the most stable state in salicylideneanilines.

UV−vis−NIR absorption was used to study how introducing acceptor−donor units changes the optical gap in COFs. First, if a COF without donor moieties such as triphenylamine was synthesized from Tf and 1,3,5-tris(4′-aminophenyl)benzene (TAPB), it exhibits an absorption edge at 465 nm with a bandgap of 2.67 eV (Figure 5c). When acceptor−donor dyad is introduced into the COF system, Tf-TAPA COF shows a redshift of the absorption peak to 595 nm (bandgap = 2.08 eV), with a broad shoulder band from 600 to 1200 nm (Figure 5c). This clearly suggests that the introduction of dyad moieties facilitates charge transfer and helps to narrow the gap. The schematic in Figure 5a explains the energy level tuning process using the dyads. In the COF with the dyad unit, the HOMO of the TPA donor segment interacts with the HOMO of the acceptor segment to create two new HOMOs. Similarly, two new LUMOs are created from donor−acceptor interactions. The energy gap is now defined by the highest HOMO and lowest LUMO among these, leading to a narrowing of the optical bandgap. While the position of the HOMO is fixed, moisture-triggered enol-keto tautomerization is expected to lower the LUMO energy level, leading to further gap narrowing. Dry Sa-TAPA COF exhibits a redshift of the absorption peak to 670 nm (bandgap = 1.85 eV) with a small shoulder band from 670 to 1200 nm (Figure 5c). The presence of the electron-withdrawing C═O groups in the *cis*-keto form helps to facilitates the charge transfer process and narrows the gap. To demonstrate the role of moisture in triggering further gap narrowing in Sa-TAPA COFs, the UV−vis−NIR absorption spectra of Tf-TAPA and Sa-TAPA COFs under different relative humidity (RH) were measured. The absorption spectra revealed no significant difference between Tf-TAPA COF that was dry or fully wetted (Figure 5c), but the absorption further red-shifted to near-infrared region at 825 nm (bandgap = 1.5 eV) for Sa-TAPA with a distinct color change from red to black when the RH exceeded 43% (Figure 5c and SI Figure S3). One explanation is the ordered porous framework structure in COF adsorbs moisture and causes a collective conformational change in the framework, this is supported by our FT−IR and solid-state CP/MAS NMR studies, where a reversible proton tautomerization in the COF backbone is triggered by exposure to moisture.

Cyclic voltammetry (CV) of the COFs was performed to determine the relative energy levels of HOMO and LUMO (Figure 5b). The working electrode was prepared by drop casting an ethanol suspension of the respective COF, carbon black, and polytetrafluoroethylene (PTFE) (2:7:1 by weight) onto a glassy carbon electrode. We could only obtain the half-cycle reduction or oxidation peaks by applying the potential to negative or positive directions because the synthesized COFs were unable to undergo reversible redox reactions and decomposed upon reduction or oxidation, As expected, Tf-TAPB COF and Tf-TAPA COF exhibit similar LUMO level (∼−3 eV) since they share the same acceptor moiety, while Tf-TAPA COF displays a higher HOMO (−4.81 eV) compared to that of Tf-TAPB (−5.5 eV) due to the introduction of triphenylamine as a donor. Notably, Sa-TAPA COF shows a significant decrease in LUMO to −3.59 eV with the incorporation of the acceptor which can undergo enol-keto tautomerization since the keto form increases its electron withdrawing ability. The bandgaps derived from CV show consistent trend with the optical gaps extracted from the absorption spectra.

Reverse saturable absorption (RSA) is a nonlinear optical property in which the material shows increasing absorption with increasing incident light intensity due to the larger excited state absorption cross-section compared to the ground state.[42]

DOI: 10.1021/acs.chemmater.8b02560
Chem. Mater. 2018, 30, 5743−5749

Such property is ideal for optical limiting applications such as protection of eyes or optical devices from laser damage. The presence of dipolar characteristics or intramolecular charge transfer is known to enhance nonlinear optical (NLO) properties, thus we expect that Sa-TAPA COF may show the same. The RSA of Sa-TAPA dispersion in acetone is confirmed by open aperture Z-scan measurement which measures the total transmittance as a function of incident laser intensity (Figure 6a). In these experiments, 532 nm nanosecond laser pulses at a very low repetition rate of 10 Hz was used to excite the sample. The Rayleigh length and the beam waist in our experiment were 1.6 mm and 17 μm, respectively. As shown in Figure 5b, the optical limiting behavior is prominent when the input laser power is larger than 0.15 GW/cm^2. The optical limiting onset value (F_{onset}, defined as the incident fluence where the optical limiting starts) is 0.77 J/cm^2, and the optical limiting threshold (F_{th}, defined as the incident fluence where the transmittance drops to 50% of the normalized linear transmittance) is 2.38 J/cm^2. These values suggest that the optical limiting response of Sa-TAPA COF is highly competitive in comparison with conventional 2D materials such as graphene and TMDCs with F_{onset} = 0.44−1.52 J/cm^2 and F_{th} = 7.2−15.15 J/cm^2.[43]

In conclusion, we have demonstrated a facile approach to engineer the bandgap of 2D COFs by introducing donor−acceptor dyads into the framework. Our studies show that molecular engineering approaches can be used to make conjugated aromatic COFs with tailor-made bandgaps. The salicylideneaniline-based triphenylamine COF, which displays moisture-triggered chromism via enol-keto tautomerization, exhibits a narrow optical gap of 1.5 eV as compared to the 2.67 eV of the COF without the dyad structure. We also show that the as-designed 2D COF with the donor−acceptor dyad exhibits excellent optical limiting behavior.

■ ASSOCIATED CONTENT

Supporting Information

The Supporting Information is available free of charge on the ACS Publications website at DOI: 10.1021/acs.chemmater.8b02560.

General information on instruments and methods; synthetic procedure of COFs; reversible proton tautomerization of small molecular salicylideneaniline; FT−IR spectra of monomers and COFs; PXRD patterns of three COFs including experimental, Pawley refinement, and simulated eclipsed and staggered stacking results; nitrogen sorption experiments of three COFs; UV−vis−NIR absorption spectra of Sa-TAPA COF under various relative humidity; SEM and TEM images of three COFs; CV of ferrocene for calibration; proposed reversible proton tautomerization of Sa-TAPA COF triggered by water; and proposed charge transfer mechanism for the humidity-triggered chromism of Sa-TAPA COF (PDF)

■ AUTHOR INFORMATION

Corresponding Authors

*E-mail: chmlyx@nus.edu.sg (Y.L.).
*E-mail: chmlohkp@nus.edu.sg (K.P.L.).

ORCID

Xing Li: 0000-0002-5470-1043
Qiang Gao: 0000-0002-8783-3245
Yixin Lu: 0000-0002-5730-166X
Kian Ping Loh: 0000-0002-1491-743X

Notes

The authors declare no competing financial interest.

■ ACKNOWLEDGMENTS

K.P.L. acknowledges NRF-CRP grant "Two Dimensional Covalent Organic Framework: Synthesis and Applications." Grant number NRF-CRP16-2015-02, funded by National Research Foundation, Prime Minister's Office, Singapore.

■ REFERENCES

(1) Feng, X.; Ding, X.; Jiang, D. Covalent organic frameworks. *Chem. Soc. Rev.* **2012**, *41*, 6010−6022.
(2) Ding, S.-Y.; Wang, W. Covalent organic frameworks (COFs): from design to applications. *Chem. Soc. Rev.* **2013**, *42*, 548−568.
(3) Jin, Y.; Hu, Y.; Zhang, W. Tessellated multiporous two-dimensional covalent organic frameworks. *Nat. Rev. Chem.* **2017**, *1*, 0056.
(4) Segura, J. L.; Mancheno, M. J.; Zamora, F. Covalent organic frameworks based on Schiff-base chemistry: synthesis, properties and potential applications. *Chem. Soc. Rev.* **2016**, *45*, 5635−5671.
(5) Diercks, C. S.; Yaghi, O. M. The atom, the molecule, and the covalent organic framework. *Science* **2017**, *355*, eaal1585.
(6) Xu, H.; Gao, J.; Jiang, D. Stable, crystalline, porous, covalent organic frameworks as a platform for chiral organocatalysts. *Nat. Chem.* **2015**, *7*, 905−912.
(7) Xu, H.-S.; Ding, S.-Y.; An, W.-K.; Wu, H.; Wang, W. Constructing Crystalline Covalent Organic Frameworks from Chiral Building Blocks. *J. Am. Chem. Soc.* **2016**, *138*, 11489−11492.
(8) Wang, X.; Han, X.; Zhang, J.; Wu, X.; Liu, Y.; Cui, Y. Homochiral 2D Porous Covalent Organic Frameworks for Heterogeneous Asymmetric Catalysis. *J. Am. Chem. Soc.* **2016**, *138*, 12332−12335.
(9) Lin, S.; Diercks, C. S.; Zhang, Y.-B.; Kornienko, N.; Nichols, E. M.; Zhao, Y.; Paris, A. R.; Kim, D.; Yang, P.; Yaghi, O. M.; Chang, C. J. Covalent organic frameworks comprising cobalt porphyrins for catalytic CO2 reduction in water. *Science* **2015**, *349*, 1208−1213.
(10) Fang, Q.; Gu, S.; Zheng, J.; Zhuang, Z.; Qiu, S.; Yan, Y. 3D Microporous Base-Functionalized Covalent Organic Frameworks for Size-Selective Catalysis. *Angew. Chem., Int. Ed.* **2014**, *53*, 2878−2882.
(11) Han, S. S.; Furukawa, H.; Yaghi, O. M.; Goddard, W. A. Covalent organic frameworks as exceptional hydrogen storage materials. *J. Am. Chem. Soc.* **2008**, *130*, 11580−11581.
(12) Furukawa, H.; Yaghi, O. M. Storage of Hydrogen, Methane, and Carbon Dioxide in Highly Porous Covalent Organic Frameworks for Clean Energy Applications. *J. Am. Chem. Soc.* **2009**, *131*, 8875−8883.
(13) Gao, Q.; Li, X.; Ning, G.-H.; Xu, H.-S.; Liu, C.; Tian, B.; Tang, W.; Loh, K. P. Covalent Organic Framework with Frustrated Bonding Network for Enhanced Carbon Dioxide Storage. *Chem. Mater.* **2018**, *30*, 1762−1768.
(14) Wan, S.; Guo, J.; Kim, J.; Ihee, H.; Jiang, D. L. A Belt-Shaped, Blue Luminescent, and Semiconducting Covalent Organic Framework. *Angew. Chem., Int. Ed.* **2008**, *47*, 8826−8830.
(15) Chen, L.; Furukawa, K.; Gao, J.; Nagai, A.; Nakamura, T.; Dong, Y.; Jiang, D. Photoelectric Covalent Organic Frameworks: Converting Open Lattices into Ordered Donor−Acceptor Heterojunctions. *J. Am. Chem. Soc.* **2014**, *136*, 9806−9809.
(16) Bessinger, D.; Ascherl, L.; Auras, F.; Bein, T. Spectrally Switchable Photodetection with Near-Infrared-Absorbing Covalent Organic Frameworks. *J. Am. Chem. Soc.* **2017**, *139*, 12035−12042.
(17) Crowe, J. W.; Baldwin, L. A.; McGrier, P. L. Luminescent Covalent Organic Frameworks Containing a Homogeneous and Heterogeneous Distribution of Dehydrobenzoannulene Vertex Units. *J. Am. Chem. Soc.* **2016**, *138*, 10120−10123.

DOI: 10.1021/acs.chemmater.8b02560
Chem. Mater. 2018, 30, 5743−5749

(18) Li, X.; Gao, Q.; Wang, J.; Chen, Y.; Chen, Z.-H.; Xu, H.-S.; Tang, W.; Leng, K.; Ning, G.-H.; Wu, J.; Xu, Q.-H.; Quek, S. Y.; Lu, Y.; Loh, K. P. Tuneable near white-emissive two-dimensional covalent organic frameworks. *Nat. Commun.* **2018**, *9*, 2335.
(19) Ding, S.-Y.; Dong, M.; Wang, Y.-W.; Chen, Y.-T.; Wang, H.-Z.; Su, C.-Y.; Wang, W. Thioether-Based Fluorescent Covalent Organic Framework for Selective Detection and Facile Removal of Mercury(II). *J. Am. Chem. Soc.* **2016**, *138*, 3031−3037.
(20) Dalapati, S.; Jin, E.; Addicoat, M.; Heine, T.; Jiang, D. Highly Emissive Covalent Organic Frameworks. *J. Am. Chem. Soc.* **2016**, *138*, 5797−5800.
(21) Gao, Q.; Li, X.; Ning, G.-H.; Leng, K.; Tian, B.; Liu, C.; Tang, W.; Xu, H.-S.; Loh, K. P. Highly photoluminescent two-dimensional imine-based covalent organic frameworks for chemical sensing. *Chem. Commun.* **2018**, *54*, 2349−2352.
(22) Montoro, C.; Rodríguez-San-Miguel, D.; Polo, E.; Escudero-Cid, R.; Ruiz-González, M. L.; Navarro, J. A. R.; Ocón, P.; Zamora, F. Ionic Conductivity and Potential Application for Fuel Cell of a Modified Imine-Based Covalent Organic Framework. *J. Am. Chem. Soc.* **2017**, *139*, 10079−10086.
(23) Ning, G.-H.; Chen, Z.; Gao, Q.; Tang, W.; Chen, Z.; Liu, C.; Tian, B.; Li, X.; Loh, K. P. Salicylideneanilines-Based Covalent Organic Frameworks as Chemoselective Molecular Sieves. *J. Am. Chem. Soc.* **2017**, *139*, 8897−8904.
(24) Huang, N.; Wang, P.; Addicoat, M. A.; Heine, T.; Jiang, D. Ionic Covalent Organic Frameworks: Design of a Charged Interface Aligned on 1D Channel Walls and Its Unusual Electrostatic Functions. *Angew. Chem., Int. Ed.* **2017**, *56*, 4982−4986.
(25) Miro, P.; Audiffred, M.; Heine, T. An atlas of two-dimensional materials. *Chem. Soc. Rev.* **2014**, *43*, 6537−6554.
(26) Nagai, A.; Chen, X.; Feng, X.; Ding, X.; Guo, Z.; Jiang, D. A Squaraine-Linked Mesoporous Covalent Organic Framework. *Angew. Chem., Int. Ed.* **2013**, *52*, 3770−3774.
(27) Chen, X.; Addicoat, M.; Jin, E.; Xu, H.; Hayashi, T.; Xu, F.; Huang, N.; Irle, S.; Jiang, D. Designed synthesis of double-stage two-dimensional covalent organic frameworks. *Sci. Rep.* **2015**, *5*, 14650.
(28) Jin, S.; Ding, X.; Feng, X.; Supur, M.; Furukawa, K.; Takahashi, S.; Addicoat, M.; El-Khouly, M. E.; Nakamura, T.; Irle, S.; Fukuzumi, S.; Nagai, A.; Jiang, D. Charge dynamics in a donor-acceptor covalent organic framework with periodically ordered bicontinuous heterojunctions. *Angew. Chem., Int. Ed.* **2013**, *52*, 2017−2021.
(29) Côté, A. P.; Benin, A. I.; Ockwig, N. W.; O'Keeffe, M.; Matzger, A. J.; Yaghi, O. M. Porous, Crystalline, Covalent Organic Frameworks. *Science* **2005**, *310*, 1166−1170.
(30) El-Kaderi, H. M.; Hunt, J. R.; Mendoza-Cortes, J. L.; Cote, A. P.; Taylor, R. E.; O'Keeffe, M.; Yaghi, O. M. Designed synthesis of 3D covalent organic frameworks. *Science* **2007**, *316*, 268−272.
(31) Liu, Y.; Ma, Y.; Zhao, Y.; Sun, X.; Gándara, F.; Furukawa, H.; Liu, Z.; Zhu, H.; Zhu, C.; Suenaga, K.; Oleynikov, P.; Alshammari, A. S.; Zhang, X.; Terasaki, O.; Yaghi, O. M. Weaving of organic threads into a crystalline covalent organic framework. *Science* **2016**, *351*, 365−369.
(32) Zhao, Y.; Guo, L.; Gándara, F.; Ma, Y.; Liu, Z.; Zhu, C.; Lyu, H.; Trickett, C. A.; Kapustin, E. A.; Terasaki, O.; Yaghi, O. M. A Synthetic Route for Crystals of Woven Structures, Uniform Nanocrystals, and Thin Films of Imine Covalent Organic Frameworks. *J. Am. Chem. Soc.* **2017**, *139*, 13166−13172.
(33) Cohen, M. D.; Flavian, S.; Leiserowitz, L. Topochemistry. Part XXVI. The absorption spectra of some thermochromic N-salicylideneanilines and hydroxynaphthylideneanilines in the crystal. *J. Chem. Soc. B* **1967**, *0*, 329−334.
(34) Ogawa, K.; Kasahara, Y.; Ohtani, Y.; Harada, J. Crystal Structure Change for the Thermochromy of N-Salicylideneanilines. The First Observation by X-ray Diffraction. *J. Am. Chem. Soc.* **1998**, *120*, 7107−7108.
(35) Harada, J.; Uekusa, H.; Ohashi, Y. X-ray Analysis of Structural Changes in Photochromic Salicylideneaniline Crystals. Solid-State Reaction Induced by Two-Photon Excitation. *J. Am. Chem. Soc.* **1999**, *121*, 5809−5810.
(36) Andes, R. V.; Manikowski, D. M. Photochromism of Salicylidene Aniline. *Appl. Opt.* **1968**, *7*, 1179−1183.
(37) de la Peña Ruigómez, A.; Rodríguez-San-Miguel, D.; Stylianou, K. C.; Cavallini, M.; Gentili, D.; Liscio, F.; Milita, S.; Roscioni, O. M.; Ruiz-González, M. L.; Carbonell, C.; Maspoch, D.; Mas-Ballesté, R.; Segura, J. L.; Zamora, F. Direct On-Surface Patterning of a Crystalline Laminar Covalent Organic Framework Synthesized at Room Temperature. *Chem. - Eur. J.* **2015**, *21*, 10666−10670.
(38) Rodriguez-San-Miguel, D.; Abrishamkar, A.; Navarro, J. A. R.; Rodriguez-Trujillo, R.; Amabilino, D. B.; Mas-Balleste, R.; Zamora, F.; Puigmarti-Luis, J. Crystalline fibres of a covalent organic framework through bottom-up microfluidic synthesis. *Chem. Commun.* **2016**, *52*, 9212−9215.
(39) Kandambeth, S.; Mallick, A.; Lukose, B.; Mane, M. V.; Heine, T.; Banerjee, R. Construction of Crystalline 2D Covalent Organic Frameworks with Remarkable Chemical (Acid/Base) Stability via a Combined Reversible and Irreversible Route. *J. Am. Chem. Soc.* **2012**, *134*, 19524−19527.
(40) Presti, D.; Labat, F.; Pedone, A.; Frisch, M. J.; Hratchian, H. P.; Ciofini, I.; Menziani, M. C.; Adamo, C. Computational Protocol for Modeling Thermochromic Molecular Crystals: Salicylidene Aniline As a Case Study. *J. Chem. Theory Comput.* **2014**, *10*, 5577−5585.
(41) Asakawa, N.; Kuroki, S.; Kurosu, H.; Ando, I.; Shoji, A.; Ozaki, T. Hydrogen-bonding effect on carbon-13 NMR chemical shifts of L-alanine residue carbonyl carbons of peptides in the solid state. *J. Am. Chem. Soc.* **1992**, *114*, 3261−3265.
(42) Tutt, L. W.; Boggess, T. F. A review of optical limiting mechanisms and devices using organics, fullerenes, semiconductors and other materials. *Prog. Quantum Electron.* **1993**, *17*, 299−338.
(43) Dong, N.; Li, Y.; Feng, Y.; Zhang, S.; Zhang, X.; Chang, C.; Fan, J.; Zhang, L.; Wang, J. Optical Limiting and Theoretical Modelling of Layered Transition Metal Dichalcogenide Nanosheets. *Sci. Rep.* **2015**, *5*, 14646.

DOI: 10.1021/acs.chemmater.8b02560
Chem. Mater. 2018, 30, 5743−5749